

Synthesis of chitosan-glutaraldehyde/activated carbon composite for methylene blue adsorption: optimization and mechanisms

Wenqian Cao, Dedong Wu*, Pengfei Xiao

College of Forestry, Northeast Forestry University, Harbin 150040, China, email: wudedong1978@126.com (D. Wu)
ORCID: 0000-0002-9152-5093; emails: 13199531169@163.com (W. Cao), xpfawd@nefu.edu.cn (P. Xiao)

Received 6 March 2022; Accepted 1 August 2022

ABSTRACT

The chitosan-glutaraldehyde/activated carbon composite (CS-G/AC) was successfully prepared as an adsorbent for methylene blue (MB)-containing wastewater. Various techniques such as Brunauer–Emmett–Teller, X-ray diffraction, Fourier-transform infrared spectroscopy, and scanning electron microscopy characterized CS-G/AC. The response surface methodology-Box–Behnken design, a method for experiments design and optimization, was employed to find the optimal MB removal conditions. The predicted maximum removal rate of MB was found to be 99.19% at an initial pH of 6.58, CS-G/AC dose of 3.2 g L⁻¹ for 35 min at 42.65°C. Compared to activated carbon (AC), the removal rate of MB by CS-G/AC increased by 44.74% at 35 min. The adsorption performance and mechanisms of CS-G/AC for MB were also investigated. Adsorption of MB onto CS-G/AC followed a pseudo-first-order kinetic model, as well as Temkin and Langmuir isothermal models with a maximum MB adsorption (Q_m) of 300.75 mg g⁻¹. Various interactions such as electrostatic interaction, π – π bonding, and hydrogen bonding were proposed as mechanisms for MB adsorption by CS-G/AC. Furthermore, CS-G/AC has been proven to be an excellent reusable adsorbent with high adsorption capacity even after six adsorption–desorption cycles. Overall, theoretical references for the preparation of CS-G/AC, treatment of MB-containing wastewater, and mechanistic analysis were provided.

Keywords: Adsorption mechanism; Chitosan-glutaraldehyde/activated carbon composite; Methylene blue; Removal rate; Response surface optimization

1. Introduction

Dyes are one of the main organic components of industrial wastewater. The textile industry is the primary contributor of dye wastewater with a 54% share [1]. During the fabric dyeing process, some dyes are not tightly bound to the fabric and tend to be carried out by water [2]. If left untreated, a negative impact on the aquatic environment and human health may occur. When the dyes enter the aquatic environment, they cause an increase in chromaticity and affect the photosynthesis of aquatic plants. The bioaccumulation

and biomagnification of these dyes also indirectly affect humans due to their consumption of aquatic foods [3,4]. Methylene blue (MB) is a thiazine dye that is one of the most commonly used cationic dyes [5]. Although MB is not particularly toxic, high doses of MB are lethal to human beings. Various negative impacts (such as dizziness, nausea, limb paralysis, and tissue gangrene) are caused by continuous MB exposure [6]. Consequently, it is imperative to find an economical and ecological method to treat high concentrations of MB-containing wastewater. Many methods have

* Corresponding author.

been recorded for the removal of MB dye. Such as adsorption [7], flocculation [8], oxidation [9], and membrane filtration [10]. Adsorption is the most prevalent because of its simplicity of operation and low energy consumption. What is crucial to the adsorption method is the adsorbent.

Therefore, based on the traditional adsorbents such as activated carbon (AC) and zeolite, numerous pieces of research have been conducted to develop new efficient adsorbents. Due to energy scarcity, adsorbent production from agricultural waste or renewable resources is becoming a trend. For instance, Zhang et al. [11] prepared a novel chestnut shell-based AC (CnSAC) for MB adsorption. The results demonstrated a maximum adsorption capacity of 500 mg g⁻¹. Alamin et al. [12] made biomass AC using *C. polygonoides* and synthesized AC-SDS microspheres with alginate under surfactant impregnation. As a result, AC-SDS was shown to have the potential for industrial use due to its high efficiency and recyclability. Besides, chitosan (CS) belongs to a naturally occurring biopolymer synthesized from chitin via a process known as N-deacetylation [13]. Owing to its widespread availability, nontoxicity, and ease of biodegradation [14], MB has been widely used in dye wastewater treatment in recent years. However, the difficulties associated with separating it from water, and its low antioxidant capacity and instability in acidic environments, have limited its use in wastewater treatment applications. Cross-linking with carbonaceous materials improves the stability of CS as well as its hydrophobicity and mechanical strength [15]. A nanocomposite was constructed using CS, montmorillonite (Mt), and polyaniline (PANI) as monomers, which outperformed other adsorbents of the same type for the adsorption of MB [16]. In addition, Men et al. developed MCS-g-PSSS to improve the adsorption selectivity of CS and facilitate adsorbent recovery. The composite achieved an adsorption capacity of 854 mg g⁻¹ for MB and was promptly separated from the system by magnetic separation [17].

Similarly, to improve the stability as well as the adsorption capacity of the adsorbent in this study, CS and AC were cross-linked with glutaraldehyde into the chitosan-glutaraldehyde/activated carbon composite (CS-G/AC). Response surface methodology (RSM) is a mathematical and statistical technique for optimizing experimental design, development, and treatment processes [18]. The Box-Behnken design (BBD) avoids extreme conditions and is highly efficient [19]. The processing conditions strongly influence CS-G/AC during the treatment of MB wastewater. Therefore, it was proposed that the response surface methodology-Box-Behnken design (RSM-BBD) be used in the study to design and optimize the MB treatment process.

The present paper was conducted to prepare CS-G/AC from single adsorbents AC and CS under water bath conditions. The prepared CS-G/AC was structurally investigated using different characterization techniques Brunauer-Emmett-Teller, X-ray diffraction (XRD), scanning electron microscopy (SEM), and Fourier-transform infrared spectroscopy (FTIR). Meanwhile, RSM-BBD was used to improve the efficiency of MB-containing wastewater treatment. The adsorption kinetics, equilibrium adsorption isotherms, the mechanisms of MB adsorption by CS-G/AC, and the regenerability of CS-G/AC were investigated.

2. Materials and methods

2.1. Materials

Chitosan (CS, C_{6n}H_{11n}NO_{4n}, Monomer MW: 161.16 g mol⁻¹, deacetylation ≥95%), methylene blue (MB, C₁₆H₁₈N₃ClS, MW: 319.86 g mol⁻¹, 99.7%, λ_{max} = 664 nm), ethanol (EtOH, >99.5%), and glutaraldehyde (C₅H₈O₂, 50%) were acquired from Aladdin Industrial Corporation (Shanghai, China). Commercial activated carbon (AC, crushed to particle size < 125 μm, 99.7%) and acetic acid (HOAc, 100%) were purchased from Hengxing Chemical Reagent Manufacturing Corporation (Tianjin, China). The pH of solutions was adjusted by hydrochloric acid (HCl) and sodium hydroxide (NaOH), which were obtained from Fengchuan Chemical Reagent Technology Corporation (Tianjin, China).

2.2. Preparation of the CS-G/AC

CS-G/AC preparation procedures were as follows: First, 12.5 g of CS was added to a beaker containing acetic acid (3%, 500 mL) with continuous stirring at 450 rpm, 70°C for 3 h in a thermostatic water bath electric stirrer (JJ-4AB, China) to obtain a CS solution. Next, according to the designed preparation conditions, appropriate amounts of CS (AC:CS = 1:1, 3:1, 5:1, 7:1, 9:1) and 50% glutaraldehyde (0.4, 0.8, 1.2, 1.6, 2.0 mL) were added to 4.2 g of pretreated AC and stirred at 450 rpm, 70°C for a specified time period (40, 80, 120, 160, 200 min). After that, the mixture was filtered through a 0.45 μm filter membrane, and the composite remaining on the membrane was collected and then washed with 0.5 mol L⁻¹ of NaOH, ethanol, and deionized water. Eventually, the synthesized CS-G/AC was dried at 50°C for 2 h before being milled into a powder and sieved through a 120-mesh sieve.

2.3. Characterization of the CS-G/AC

The specific surface area and pore volume of AC and CS-G/AC were determined using the Micromeritics ASAP 2460 analyzer at 77 K using nitrogen adsorption/desorption isotherms. X-ray powder diffraction patterns of AC, CS-G/AC, and regenerated CS-G/AC were obtained by an X-ray diffractometer (XRD, D8 ADVANCE, Germany). Scanning electron microscopy (SEM, SU-8020, Japan) was employed to observe the morphology and microstructure of AC and CS-G/AC. Fourier-transform infrared spectroscopy (FTIR, Nicolet IS10, United Kingdom) was utilized to determine the functional groups on the surface of AC, CS, and CS-G/AC before and after MB adsorption. The zero point of charge (pH_{pzc}) of CS-G/AC measurement was performed according to the paper to determine the surface charge of CS-G/AC [20].

2.4. Single factor test

For each experiment, CS-G/AC was added to a 250 mL beaker along with 100 mL MB simulated wastewater (200 mg L⁻¹). All experiments were performed in an ultrasonic cleaner (SB25-12DTD, China), shaking at 300 W for a certain time. The single-factor tests were conducted with four factors: treatment temperature (15°C, 25°C, 35°C, 45°C,

55°C), initial pH (3.5, 4.5, 5.5, 6.5, 7.5), adsorbent dose (1.0, 1.6, 2.2, 2.8, 3.4 g L⁻¹), and treatment time (5, 15, 25, 35, 45 min). Each MB removal experiment was replicated three times, and one-way ANOVA was performed using SPSS 21.0 software.

2.5. Experiment design and optimization

Design-Expert 12.0 was used to design the experiments, and a primary relationship between evaluation responses was developed and analyzed using the data from 17 design points. The factor levels used in the BBD model are listed in Table 1. The removal rate of MB was predicted, and the experimental data were analyzed using a quadratic equation, as follows (1) [21]:

$$Y = k_0 + \sum_{i=1}^n k_i X_i + \sum_{i=1}^n k_{ii} X_i^2 + \sum_{i=1}^n \sum_{j=i+1}^n k_{ij} X_i X_j \tag{1}$$

where Y (%) is the predicted response to MB removal, X_i and X_j are independent variables, k₀, k_i, k_{ii} and k_{ij} are model constants, the linear regression coefficient, the quadratic term coefficient, and the interaction coefficient. Typically, the BBD model generates 17 runs.

Table 2 contains the actual experimental design matrix and values for MB removal.

2.6. Adsorption study

0.5 g L⁻¹ of CS-G/AC was added to 100 mL of MB simulated wastewater for the adsorption experiment. The adsorption experiment was performed at various contact times (0–110 min) and initial concentrations (20, 40, 60, 80, 100, 150, 200 mg L⁻¹), respectively, in the optimum state. Then, CS-G/AC was removed with a filter membrane

(0.45 μm). The initial and final concentrations of MB were measured by UV spectrophotometry at a wavelength of 664 nm. The amount of MB adsorption at a specific time, q_t (mg g⁻¹), was calculated by Eq. (2).

$$q_t = (C_0 - C_t) \times \frac{V}{M} \tag{2}$$

where V (L) and M (g) represent the volume of MB solution and mass of CS-G/AC, respectively.

3. Results and discussion

3.1. Effect of preparation conditions on MB removal by CS-G/AC

Fig. 1 depicts the impacts of cross-linking time, the mass ratio of AC and CS, and the amount of 50% glutaraldehyde on MB removal and adsorption capacity of the prepared CS-G/AC, respectively.

As seen in Fig. 1, the removal rate of MB increased and then decreased with the increase of cross-linking time, the mass ratio of AC and CS, and the amount of 50% glutaraldehyde. Adsorption capacity showed the same trend as the removal rate. From Fig. 1a, when cross-linked for

Table 1
Experimental variables and their coded levels

Factors	Coding level		
	-1	0	1
A: initial pH	5.5	6.5	7.5
B: adsorbent dose (g L ⁻¹)	2.2	2.8	3.4
C: temperature (°C)	35	45	55

Table 2
The 3-variables BBD matrix and experimental data for MB removal

Run	A: initial pH	B: adsorbent dose (g L ⁻¹)	C: temperature (°C)	MB removal rate (%)
1	7.5	3.4	45	98.19
2	6.5	2.8	45	98.93
3	6.5	2.8	45	98.99
4	5.5	2.2	45	93.09
5	7.5	2.2	45	97.33
6	6.5	2.8	45	98.79
7	6.5	2.2	35	93.34
8	7.5	2.8	35	97.62
9	6.5	3.4	35	98.82
10	5.5	3.4	45	97.95
11	6.5	2.2	55	97.5
12	7.5	2.8	55	97.62
13	5.5	2.8	35	96.78
14	6.5	2.8	45	98.84
15	6.5	3.4	55	98.03
16	5.5	2.8	55	97.23
17	6.5	2.8	45	98.04

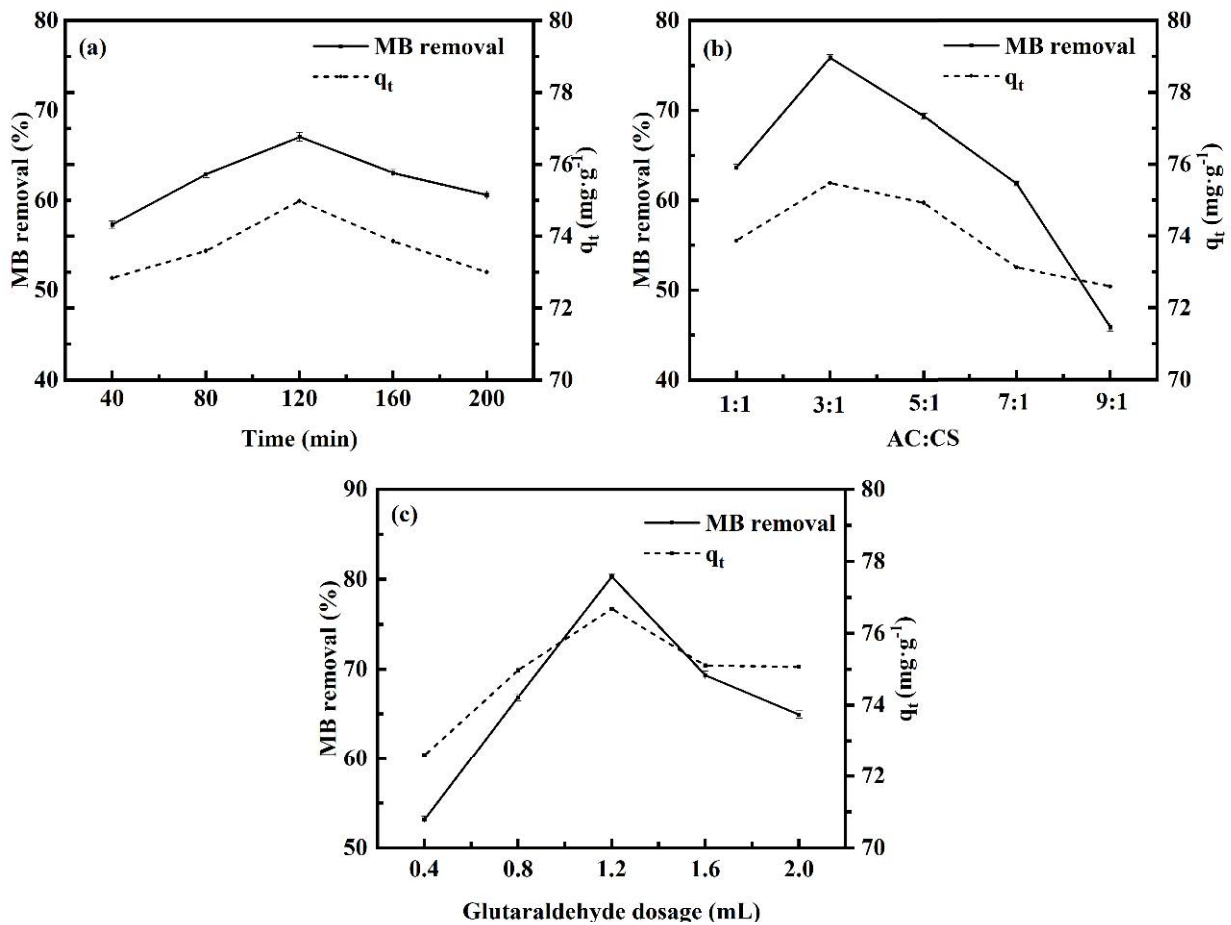


Fig. 1. Effect of (a) time (min), (b) AC:CS, (c) glutaraldehyde dosage (mL) on MB removal and q_t of prepared CS-G/AC. (Temperature = 40°C; CS-G/AC dosage = 2.5 $\text{g}\cdot\text{L}^{-1}$; initial pH = 5.5; ultrasonic power = 300 W; treatment time = 20 min).

120 min, the removal rate of MB reached a maximum value of 67.04%, and the adsorption capacity was 74.98 $\text{mg}\cdot\text{g}^{-1}$, remarkably higher than the other cross-linking times ($P < 0.05$). As the cross-linking time increased, adequate contact and cross-linking between CS and AC were facilitated. However, prolonged cross-linking time made CS-G/AC over cross-linked, resulting in the stacking phenomenon and decreased specific surface area, reducing its adsorption ability. The maximum removal rate and adsorption capacity of MB, 75.86% ($P < 0.05$), and 75.48 $\text{mg}\cdot\text{g}^{-1}$ occurred at a mass ratio of AC to CS of 3:1. Both AC and CS possessed adsorption properties, and when cross-linked at the proper mass ratio, the adsorption capacity was enhanced [22]. When 1.2 mL 50% glutaraldehyde was added to the system, the maximum MB removal rate of 80.30% ($P < 0.05$) and q_t of 76.68 $\text{mg}\cdot\text{g}^{-1}$ were obtained. Low MB adsorption due to low glutaraldehyde dosage was attributed to incomplete cross-linking. When the cross-linking agent overdosed, the MB adsorption process was disturbed by the non-functional glutaraldehyde on the surface of CS-G/AC [23].

In summary, CS-G/AC prepared under 120 min of cross-linking time, 3:1 mass ratio of AC and CS, and 1.2 mL of glutaraldehyde dosage conditions were selected for the subsequent tests.

3.2. Comparison of AC and CS-G/AC for MB removal performance

The comparison of MB removal performance between AC and CS-G/AC is shown in Fig. 2. The removal rate of MB by CS-G/AC reached 78.9% after 50 min treatment, while AC reached 44.12%. Under the same processing conditions, the difference in the removal rate of MB between AC and CS-G/AC varied with time. In the first 15 min, the difference increased rapidly with time, then increased at a slower rate between 15 and 35 min, and finally reached a maximum value of 44.74% at 35 min.

The CS-G/AC developed in this study outperformed AC for MB removal.

3.3. Characterization of the CS-G/AC

3.3.1. N_2 adsorption/desorption isotherms and pore-size distribution

The N_2 adsorption/desorption curves and pore-size distributions of AC and CS-G/AC are presented in Fig. 3. Based on the IUPAC classification, both AC and CS-G/AC isotherms can be classified as type IV with H4-type hysteresis loop ($P/P_0 < 0.5$), indicating the presence of mesoporous structures [24]. The specific surface area, total

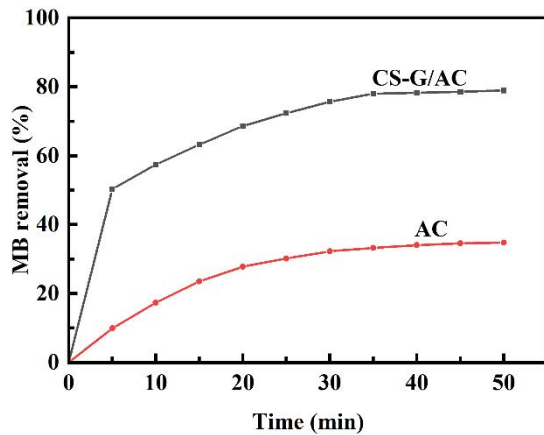


Fig. 2. Ability of CS-G/AC vs. AC for MB removal.

pore volume, and adsorption average pore size of AC were $48.47 \text{ m}^2 \text{ g}^{-1}$, $0.04 \text{ cm}^3 \text{ g}^{-1}$, and 3.38 nm , respectively, whereas the specific surface area, total pore volume, and adsorption average pore size of CS-G/AC were $8.1 \text{ m}^2 \text{ g}^{-1}$, $0.02 \text{ cm}^3 \text{ g}^{-1}$, and 7.81 nm , respectively. Compared to AC,

the specific surface area of CS-G/AC decreased due to the partial blockage of pores by CS.

3.3.2. XRD analysis

The XRD profiles of AC, CS-G/AC, and regenerated CS-G/AC are shown in Fig. 4. From Fig. 4, the presence of two broad peaks at 2θ values of 25° and 40° were observed, which were attributed to the presence of amorphous and graphitic carbon structures [25]. After the cross-linking of AC with CS, the characteristic peak of CS appeared at $2\theta = 10^\circ$ [26], and the peak of CS-G/AC was wider than AC, indicating that CS was successfully cross-linked with AC. Except for a slight change in peak intensity, there was little change in the peak width of the regenerated CS-G/AC, indicating that CS-G/AC was recyclable.

3.3.3. Fourier-transform infrared spectroscopy

The FTIR spectra of CS, AC, CS-G/AC, and regenerated CS-G/AC are depicted in Fig. 5. The bands at $2,923.10$; $1,631.63$ and $1,384.71 \text{ cm}^{-1}$, respectively, represented the C–H stretching vibration, the N–H bending vibration, and the symmetric bending vibration peak of $-\text{CH}_3$ [27].

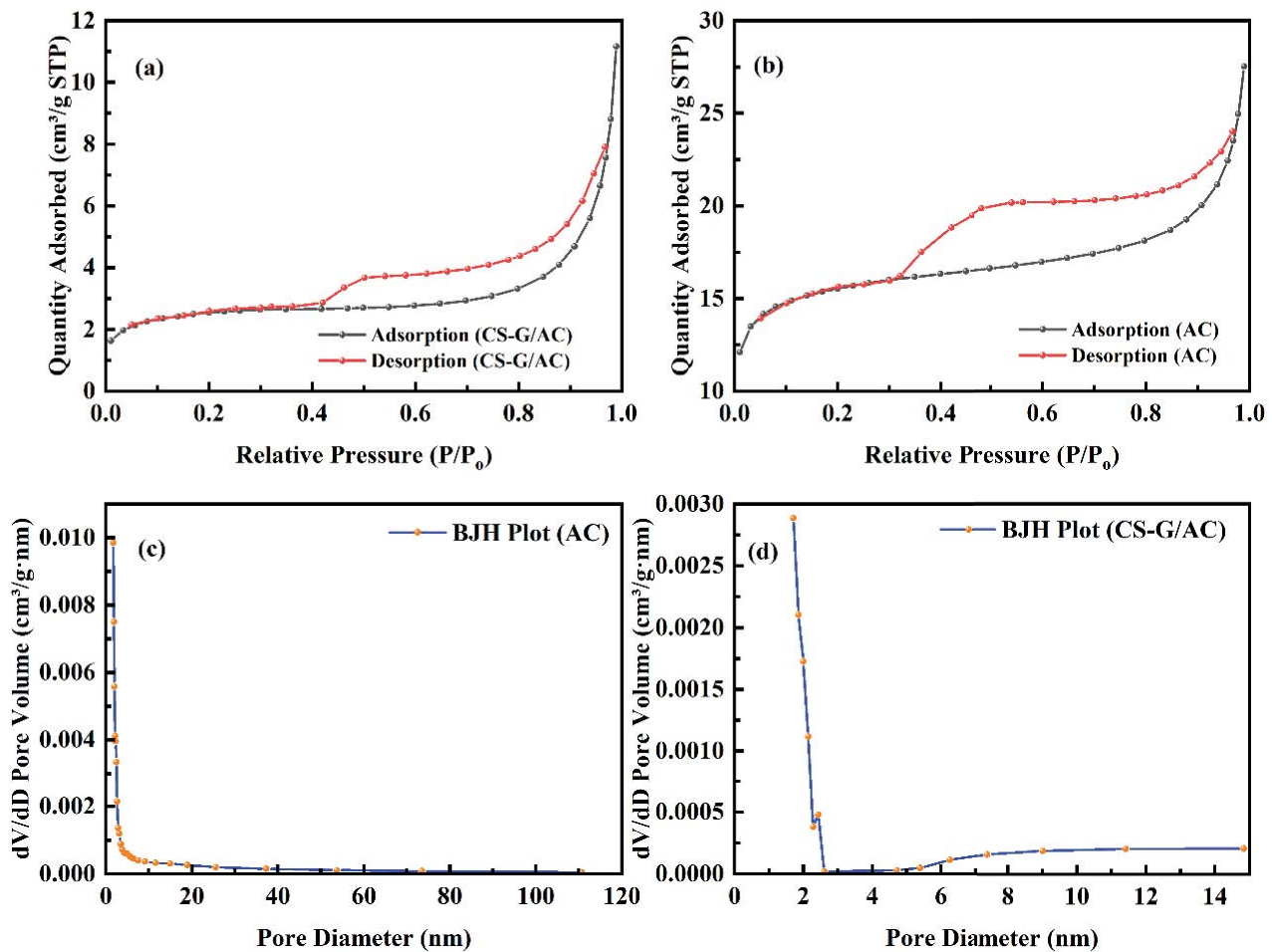


Fig. 3. N_2 adsorption/desorption isotherms and pore-size distribution of AC and CS-G/AC.

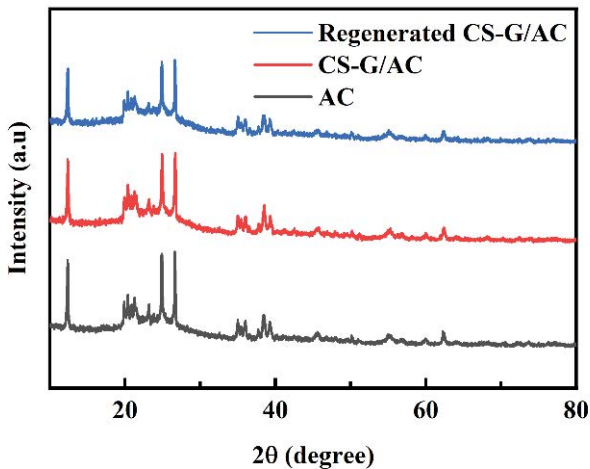


Fig. 4. XRD patterns of AC, CS-G/AC and regenerated CS-G/AC.

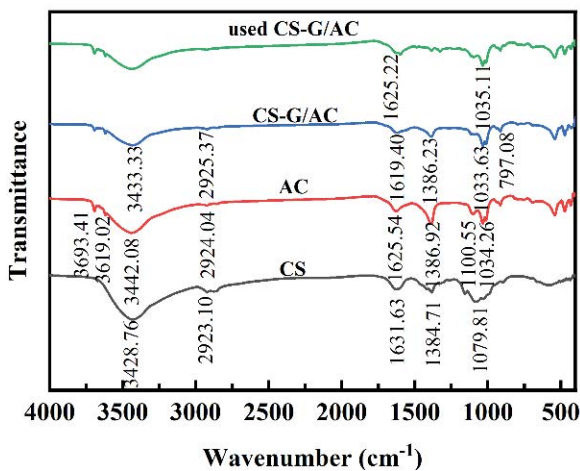


Fig. 5. FTIR spectra of CS, AC, CS-G/AC, and CS-G/AC after MB adsorption.

These characteristic peaks were retained in the composite due to the cross-linking of CS and AC. The N–H bending vibration peak at $1,631.63\text{ cm}^{-1}$ strengthened and shifted towards the lower wavenumber to $1,619.40\text{ cm}^{-1}$; the C–H stretching vibration at $2,923.10\text{ cm}^{-1}$ and the $-\text{CH}_3$ symmetric bending vibration at $1,384.71\text{ cm}^{-1}$ weakened, and the two vibration peaks moved to $2,925.37$ and $1,386.23\text{ cm}^{-1}$, respectively [28]. Moreover, it was found that the composite exhibited a C–C vibrational peak representing the characteristic carbohydrate skeleton at 797.09 cm^{-1} in comparison to AC, indicating the successful cross-linking of CS and AC [29]. Additionally, the cross-linking of AC and CS strengthened the carboxylic acid's C=O stretching vibration at $3,442.08\text{ cm}^{-1}$ in AC and weakened the $-\text{OH}$ stretching vibration at $3,428.08\text{ cm}^{-1}$ in CS, resulting in the formation of a new vibrational peak at $3,433.33\text{ cm}^{-1}$ in composite, indicating the presence of C=O---H–O hydrogen bonding between CS and AC [30]. The composite's IR band of $-\text{OH}$ was shifted, broadened, and attenuated in $3,700\text{--}3,200\text{ cm}^{-1}$, indicating the presence of hydrogen bonds [31]. The density

of the minor peaks in the range of $600\text{--}1,000\text{ cm}^{-1}$ confirmed the presence of aromatic rings [32]. The waveforms of CS-G/AC before and after the MB adsorption were similar. However, many spurious peaks appeared in the $1,625.22\text{--}1,035.11\text{ cm}^{-1}$ band, which may be influenced by the $\pi\text{--}\pi$ stacking effect of CS-G/AC and MB [33]. That indicated the successful adsorption of MB by CS-G/AC.

3.3.4. Scanning electron microscopy

As presented in Fig. 6, SEM analysis was used to investigate the morphology of AC and CS-G/AC. As seen in Fig. 6a, the surface of AC was relatively smooth with few pores and cracks. While in Fig. 6b, CS-G/AC had a greater abundance of pore-like structures, cracks, and depressions than AC. Additionally, the random distribution of CS on the composite surface not only created the appearance of multiple shell-shaped structures but also roughened the surface of the composite.

3.4. Single-factor experiment analysis

Fig. 7 shows the impacts of temperature, initial pH, adsorbent dose, and treatment time on the MB removal and adsorption capacity of CS-G/AC, respectively.

3.4.1. Effect of temperature

From Fig. 7a, the treatment capacity of the CS-G/AC for MB gradually increased as the temperature rose. The removal rate of MB was 88.33% at 55°C ($P < 0.05$), and q_t was 77.18 mg g^{-1} . However, after 45°C , further increasing the temperature did not effectively improve the treatment of MB. Furthermore, the desorption of MB from composite containing AC and CS was an endothermic process [34]. MB might desorb from the composite surface and diffuse into the solution as the temperature increases. 45°C was chosen as the optimum treatment temperature when energy saving was taken into account.

3.4.2. Effect of initial pH

It can be seen from Fig. 7b that the removal rate and q_t of MB increased with the initial pH from 3.5 to 6.5 and decreased beyond 6.5. Therefore, the initial pH of 6.5 was selected for the following step. The removal rate and q_t of MB were 93.37% and 78.43 mg g^{-1} , respectively. In an alkaline environment, the electronegativity of the N atom of MB was reduced, which made the cationic nature of the dye less pronounced. Consequently, electrostatic interaction was weakened. Furthermore, under weak acid condition, the formation of hydroxyl groups on the surface of AC was facilitated, which increased the effective surface area for MB adsorption [35].

3.4.3. Effect of adsorbent dose

From Fig. 7c, the effect of adsorbent dose on the removal rate of MB exhibited a similar trend to that of temperature. When the adsorbent dosage increased from 1 to 2.8 g L^{-1} , the removal rate of MB increased by 41.33% . At adsorbent

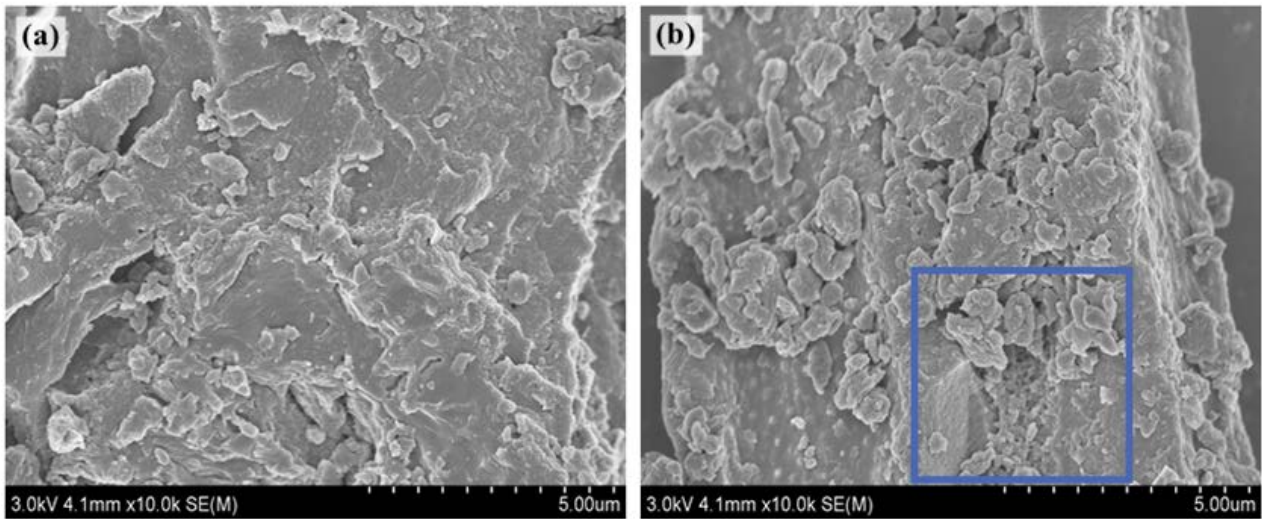


Fig. 6. SEM analysis of (a) AC and (b) CS-G/AC.

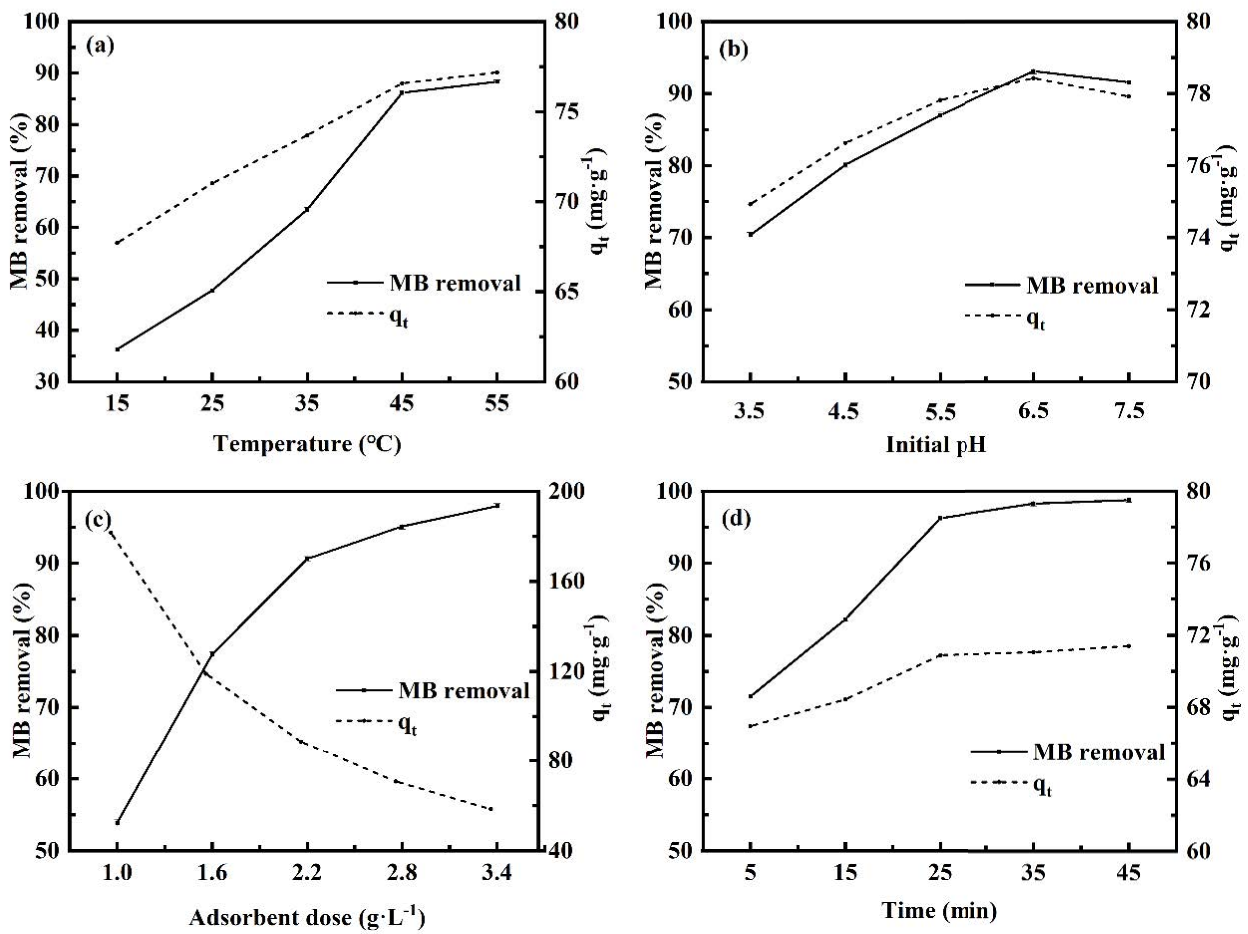


Fig. 7. Removal rate and q_t of MB varies with the following parameters: (a) temperature (°C), (b) initial pH, (c) adsorbent dose (g L⁻¹), and (d) time (min). (Temperature = 40°C; CS-G/AC dosage = 2.5 g L⁻¹; initial pH = 5.5; ultrasonic power = 300 W; treatment time = 20 min).

dosage above 2.8 g L⁻¹, the removal rate of MB changed slightly. Excessive adsorbent addition may lead to saturation of the solution with adsorbent, giving rise to vacant adsorption sites and reduced adsorption capacity [36]. However, as the adsorbent dose increased, the free adsorption sites on the CS-G/AC surface were reduced rapidly due to the high accumulation of adsorbents. An adsorbent dosage of 2.8 g L⁻¹ was selected for further study.

3.4.4. Effect of treatment time

From Fig. 7d, the removal rate of MB increased significantly ($P < 0.05$) from 71.57% to 98.27% as the treatment time increased from 5 to 35 min. However, the removal rate did not improve by increasing the treatment time further. Adsorption capacity showed the same trend. The longer the treatment time, the greater the chance of collision between MB and the composite. However, after an extended treatment time, MB ions adsorbed on the surface of the composite tend to repel the MB ions in the solution, resulting in the ineffective use of remaining adsorption sites. In the follow-up study, 35 min was determined to be the reaction time.

Above all, three factors: initial pH (A), adsorbent dose (B), and temperature (C), which had the most significant effect on MB removal, were selected in the RSM-BBD analysis.

3.5. RSM-BBD analysis

As displayed in Table 3, analysis of variance (ANOVA) was utilized to analyze the MB removal results. The BBD model had an F -value of 11.71 and a corresponding P -value of (<0.05). Therefore, the statistical significance of the BBD model for MB removal was revealed. The F -value was 5.34, and the P -value in the misfit term was 0.0697. This result indicated that the misfit was insignificant

and that the model accurately predicted the conditions under which the MB was removed. The model correlation coefficient ($R^2 = 0.9442$) originated from the selected variables, accounting for 94.42% of the removal rate of MB. Besides, all terms except C, AC, and C² were significant in removing MB. The F -value is used to determine the significance of variables' effects on the removal rate of MB. The greater the F -value, the more significant the effect. As a result, the independent variables' intensity sequence was as follows: $B > A > C$.

3.6. Influence and interactions of various factors

The 3D response surfaces between initial pH, adsorbent dose, and temperature are given in Fig. 8. As illustrated in Fig. 8a, the response surface was relatively steep, indicating that the initial pH and adsorbent dose had significant interaction. Moreover, the 3D plot demonstrated that as the initial pH value increased, the removal rate of MB increased rapidly and then began a downward trend after reaching about 6.5. The removal rate of MB kept increasing from 2.2 to 3.4 g L⁻¹, although the increasing rate tapered off in the later stage. MB's most incredible removal rate was attained at an initial pH of roughly 6.5 and an adsorbent dosage of around 3.2 g L⁻¹. According to Fig. 8b, a flat response surface suggested no significant interaction between initial pH and temperature. The highest removal rate of MB occurred at an initial pH of 6.5 and a temperature of 43°C. From Fig. 8c it could be observed that there was a steep response surface, which indicated a significant interaction between adsorbent dose and temperature. The removal rate of MB increased steadily as the temperature increased from 35°C to 45°C, peaking at around 43°C. When the temperature was held constant, the removal rate of MB rose with the adsorbent dose, and the curved surface showed a tendency to rise rapidly and then slowly, reaching the

Table 3
ANOVA for the removal of MB

Source	df	Sum of squares	Mean square	F -value	P -value	Sig.
Model	9	45.12	5.01	11.71	<0.05	*
A	1	4.08	4.08	9.52	0.0177	*
B	1	17.20	17.20	40.19	0.0004	**
C	1	1.82	1.82	4.26	0.0778	NS
AB	1	4.00	4.00	9.35	0.0184	*
AC	1	0.05	0.05	0.12	0.7410	NS
BC	1	6.13	6.13	14.32	0.0069	**
A ²	1	3.00	3.00	7.01	0.0331	*
B ²	1	6.41	6.41	14.98	0.0061	**
C ²	1	1.33	1.33	3.10	0.1216	NS
Residual	7	3.00	0.43			
Lack of fit	3	2.40	0.80	5.34	0.0697	NS
Pure error	4	0.60	0.15			
Cor. total	16	48.11				

where “***” indicates a highly significant difference ($P < 0.01$);

“**” where represents a significant difference ($P < 0.05$);

“NS” means a non-significant difference.

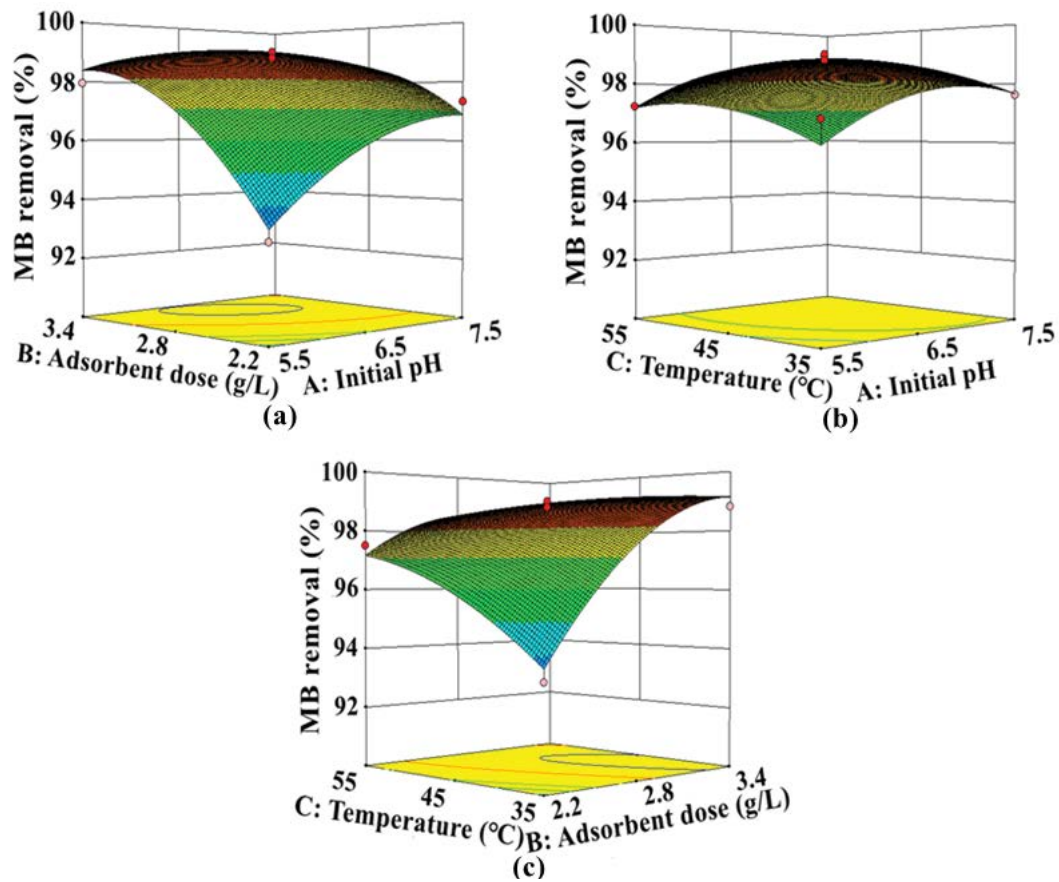


Fig. 8. 3D response surface plot of MB removal revealing the interaction between: (a) initial pH and adsorbent dose, (b) initial pH and temperature, and (c) adsorbent dose and temperature.

ideal value around the dosage of 3.2 g L^{-1} . The maximum amount of MB was adsorbed on the surface of CS-G/AC at 45°C and an adsorbent dose of 3.2 g L^{-1} . In conclusion, the interactions between the three factors affecting the removal rate of MB were as follows: $BC > AB > AC$.

3.7. Process interaction

The relationship between the independent variables and the removal rate of MB was realized by a second-order polynomial Eq. (3) as follows:

$$Y(\%) = 98.72 + 0.71A + 1.47B + 0.48C - AB - 0.11AC - 1.24BC - 0.84A^2 - 1.23B^2 - 0.56C^2 \quad (3)$$

By solving the regression equation above, the optimal conditions for treatment MB by CS-G/AC were determined as follows: With an initial pH of 6.58, a dose of 3.2 g L^{-1} adsorbent, a temperature of 42.65°C , and a treatment time of 45 min, the predicted removal rate of MB was 99.19%. Three replicate experiments under optimal conditions were conducted to verify the accuracy of the predictions, and the average removal rate of MB was 98.93%. The results indicated that optimizing the MB treatment process using RSM utilizing the prepared composite was reasonable and feasible.

3.8. Equilibrium adsorption study

In Fig. 9a the adsorption capacity of CS-G/AC vs. time at different initial concentrations of MB was shown. The composite showed a large increase in adsorption during the first 30 min of treatment, followed by a slow increase. CS-G/AC reached adsorption equilibrium at all the above concentrations at 40 min. Besides, the equilibrium adsorption capacity of CS-G/AC towards MB increased from 36.33 to 274.93 mg g^{-1} as the initial concentration increased from 20 to 200 mg L^{-1} . The mass transfer driving force was proportional to the difference in concentration of MB between the solution and the CS-G/AC surface, so the adsorption rate was fast in the first 20 min. With increasing treatment time, the concentration difference decreased gradually, and the mass transfer driving force weakened [37], leading to a lower adsorption rate in the latter part of the treatment.

3.9. Adsorption kinetics

The pseudo-first-order and non-linear pseudo-second-order kinetic models were used to fit experimental data of CS-G/AC adsorption of MB at various initial concentrations in this study. The nonlinear equations for pseudo-first-order and pseudo-second-order are shown in Eqs. (4) and (5), respectively [38].

$$\ln(q_e - q_t) = \ln q_e - k_1 t \quad (4)$$

$$\frac{t}{q_t} = \frac{1}{k_2 q_e} + \frac{t}{q_e} \quad (5)$$

where q_t (mg g^{-1}) and q_e (mg g^{-1}) denote the amount of MB absorbed by CS-G/AC at time t (min) and equilibrium, respectively. k_1 (min^{-1}) and k_2 ($\text{g mg}^{-1} \text{min}^{-1}$) represent the rate constants of pseudo-first-order and pseudo-second-order, respectively.

The relevant parameters of the kinetic model are summarized in Table 4. For various initial MB concentrations, the R^2 of the pseudo-first-order model was greater, and the calculated q_e ($q_{e,\text{cal}}$) was closer to the experimental value ($q_{e,\text{exp}}$) compared to the fitted results of the pseudo-second-order model. The pseudo-first-order model was proved to be more suitable for describing the adsorption process of CS-G/AC on MB. The adsorption process was dominated by physical adsorption [39].

3.10. Adsorption isotherms

Adsorption isotherms can be used to investigate the type of interaction between MB and CS-G/AC and gain a better theoretical understanding of the adsorption mechanism. The nonlinear equilibrium model of Langmuir, Freundlich, and Temkin was employed to fit the experimental data to evaluate the adsorption capacity of CS-G/AC for MB. Eqs. (6)–(8), respectively, show the nonlinear equations for these models [40–42]:

$$\frac{C_e}{q_e} = \frac{1}{K_L Q_m} + \frac{t}{Q_m} \quad (6)$$

$$q_e = K_F C_e^{\frac{1}{n}} \quad (7)$$

$$q_e = \frac{RT \ln(K_T C_e)}{b_T} \quad (8)$$

where q_e (mg g^{-1}) represents the adsorption capacity of CS-G/AC on MB, C_e (mg L^{-1}) is the amount of residual MB

after adsorption at equilibrium, Q_m (mg g^{-1}) is the theoretical maximum adsorption capacity of CS-G/AC on MB, K_L (L mg^{-1}), K_F (L g^{-1}), and K_T (L g^{-1}) are the isothermal model constraints, n is the adsorption strength, b_T (kJ mol^{-1}) is the absorption heat, T (K) is the temperature, R ($8.314 \text{ kJ mol}^{-1} \text{K}^{-1}$) is the gas constant. The parameters of the nonlinear curves and isotherms are presented in Fig. 9b and Table 5, respectively.

According to the correlation coefficient R^2 analysis shown in Table 5, both the Langmuir and Temkin isothermal models had a high R^2 (>0.90), indicating the adsorption of MB dye on the CS-G/AC surface occurred as single-layer adsorption [43]. Moreover, it can be deduced that an electrostatic adsorption process occurred during the MB adsorption by CS-G/AC [44].

At 316 K, the maximum adsorption of CS-G/AC on MB was 300.75 mg g^{-1} . On the one hand, ion-exchange mechanisms possessed b_T values of 8 to 16 kJ mol^{-1} , whereas physisorption processes had b_T values of less than 40 kJ mol^{-1} . The b_T values obtained in this study did not lie within these two ranges, implying that the adsorption process involved both chemisorption and physisorption [45]. On the other hand, the value of K_L obtained from the Langmuir model fit was 0.1458, which was within the range of 0 to 1, demonstrating that the adsorption process was easy to perform [46].

3.11. Regeneration of CS-G/AC

To investigate the effect of regeneration times on the adsorption of MB by CS-G/AC, the used composite was washed with deionized water to remove surface impurities. The solution was then desorbed with ethanol and sonicated

Table 5
Parameters of isotherm models for MB onto CS-G/AC

Model	Parameters		
Langmuir	Q_m (mg g^{-1})	K_L (L mg^{-1})	R^2
	300.75	0.1458	0.9240
Freundlich	K_F (L g^{-1})	$1/n$	R^2
	67.2704	0.3559	0.8722
Temkin	K_T (L g^{-1})	b_T (kJ mol^{-1})	R^2
	2.7183	41.272	0.9284

Table 4
Parameters of adsorption kinetic models for MB onto CS-G/AC

Concentrations (mg L^{-1})	$q_{e,\text{exp}}$ (mg g^{-1})	Pseudo-first-order			Pseudo-second-order		
		$q_{e,\text{cal}}$ (mg g^{-1})	k_1 (min^{-1})	R^2	$q_{e,\text{cal}}$ (mg g^{-1})	k_2 ($\text{g mg}^{-1} \text{min}^{-1}$)	R^2
20	36.33	36.63	0.1004	0.9981	40.75	0.0035	0.9802
40	73.56	72.63	0.1468	0.9924	78.41	0.0031	0.9956
60	113.45	110.37	0.1942	0.9816	117.73	0.0030	0.9982
80	151.89	151.09	0.1355	0.9924	163.68	0.0014	0.9900
100	175.67	174.15	0.1942	0.9977	184.79	0.0020	0.9938
150	242.59	238.61	0.1093	0.9723	261.73	0.0006	0.9868
200	274.93	270.68	0.2732	0.9912	282.93	0.0021	0.9987

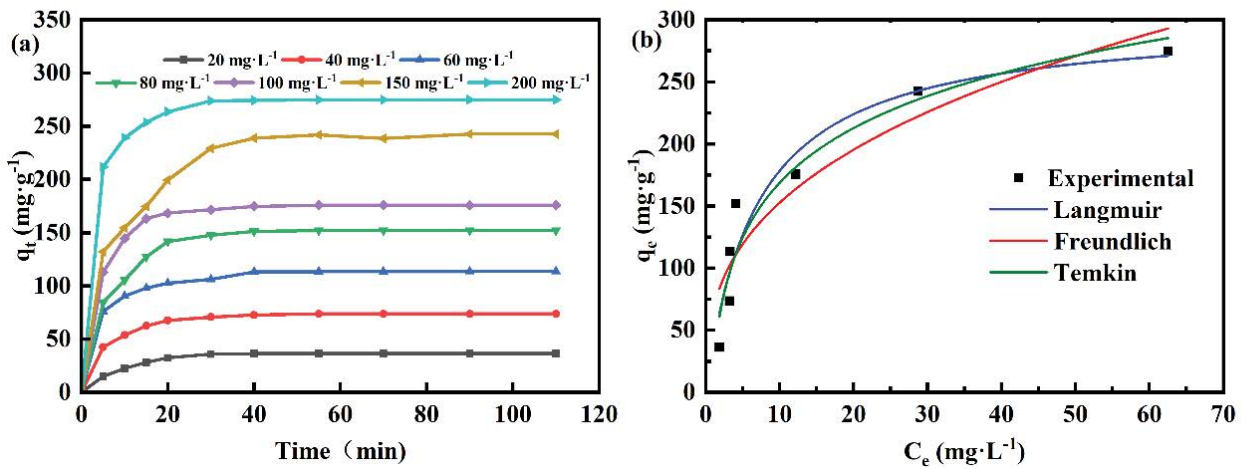


Fig. 9. (a) Effect of contact time on MB adsorption at different initial concentrations and (b) adsorption isotherms of MB by CS-G/AC (solution pH = 6.58; adsorbent dose = 0.5 g L⁻¹; temperature = 316 K; ultrasonic power = 300 W; volume of solution = 100 mL).

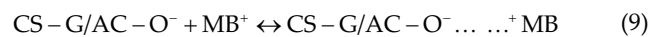
at 540 W, 20°C, until MB was undetectable in the filtrate. After elution, the regenerated material was washed several times with deionized water to eliminate the effect of ethanol. The regenerated CS-G/AC was then used for the next cycle. The effect of regeneration times on the adsorption capacity of CS-G/AC is shown in Fig. 10. As shown in Fig. 10, after six regenerations, CS-G/AC maintained a high adsorption capacity of 68.17 mg g⁻¹ for MB, 89.65% of the first adsorption capacity. It was confirmed that the material was reusable.

3.12. Adsorption mechanism

The mechanism of MB adsorption on CS-G/AC is shown in Fig. 11.

CS-G/AC showed amphoteric properties. The charge on the surface varies with the pH value of the solution. CS-G/AC had a pH_{pzc} of 6.43, as shown in Fig. 12. When the solution $pH > pH_{pzc}$, the CS-G/AC surface was negatively charged; the composite surface was positively charged when the solution pH was less than pH_{pzc} . As a result, at

initial $pH = 6.58$ ($pH > pH_{pzc}$), the surface charge of CS-G/AC was negative, and electrostatic attraction between CS-G/AC and the cationic dye MB occurred, which was considered the main role in the adsorption of MB on the surface of CS-G/AC [47]. The electrostatic attraction between MB and CS-G/AC is shown in Eq. (9):



Furthermore, FTIR plots showed that the $\pi-\pi$ bond formed between CS-G/AC and MB increased the MB absorption. Additionally, hydrogen bonds between the donor hydrogen sites on the surface of CS-G/AC and the oxygen and nitrogen in the MB molecules also worked.

Table 6 shows the comparison of CS-G/AC with other adsorbents used for MB adsorption. Table 6 revealed that CS-G/AC prepared in this study had a stronger adsorption capacity than biochar and is superior to most modified AC. Additionally, AC and CS were non-toxic, non-hazardous, and widely available. Therefore, CS-G/AC was a promising and efficient adsorbent for MB adsorption.

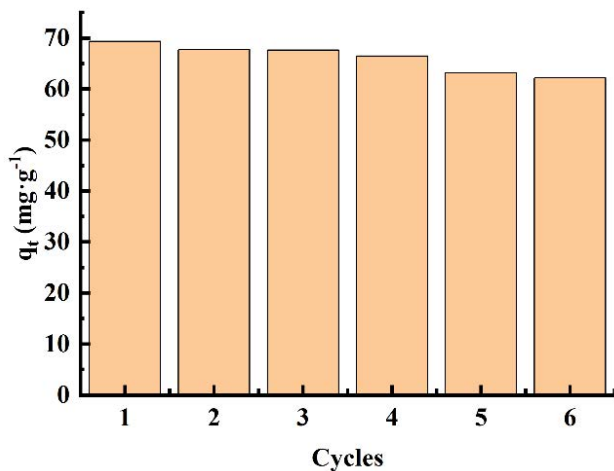


Fig. 10. Effect of regeneration times on the adsorption performance of CS-G/AC.

Table 6
Comparison of the adsorption capacity of MB by various adsorbents

Adsorbent	Q_m (mg g ⁻¹)	References
CS-G/AC	300.75	This study
ACSO/Fe ₃ O ₄ magnetic composite	60.6	[48]
Peanut shell biochar	225.8	[49]
Hickory biochar	16	[50]
Carboxymethyl cellulose/Fe ₃ O ₄	83.6	[51]
NaOH-modified tea biochar	67.29	[52]
Mesoporous Iraqi red kaolin clay	240.4	[53]
Carrageenan and itaconic acid-based super-adsorbent hydrogel	2,439.02	[54]

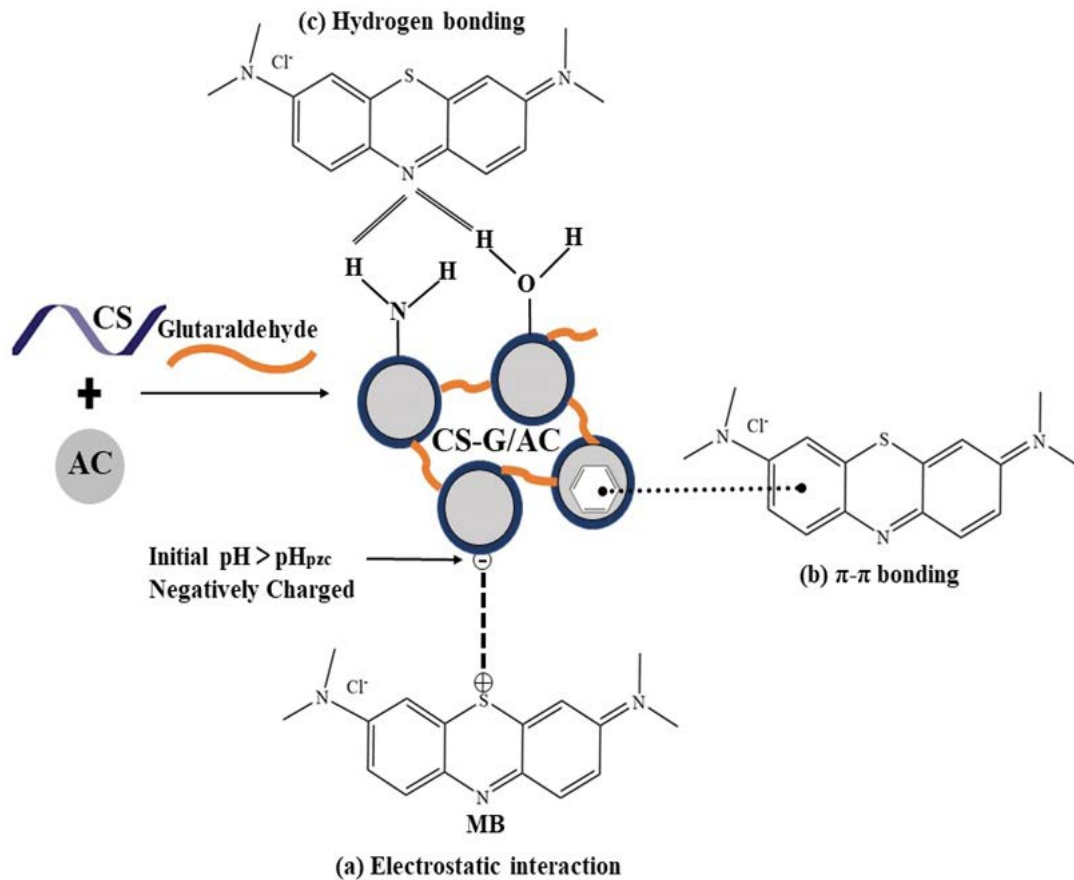


Fig. 11. Illustration of possible mechanisms for MB adsorption by CS-G/AC: (a) electrostatic interaction, (b) π - π bonding, and (c) hydrogen bonding.

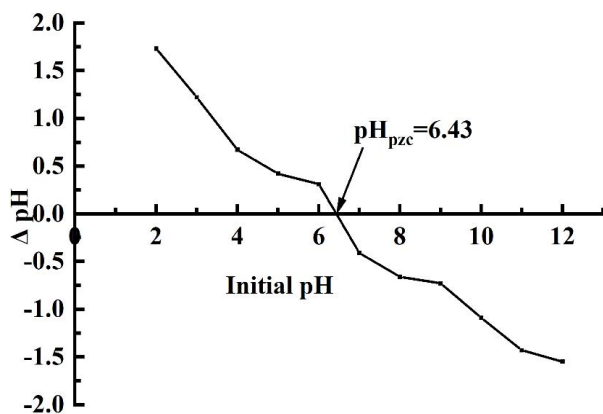


Fig. 12. pH_{pzc} of CS-G/AC.

4. Conclusions

In this work, CS-G/AC was successfully prepared and implemented in simulated wastewater containing MB. CS-G/AC with a cross-linking time of 120 min, a mass ratio of AC to CS of 3:1, and a 50% glutaraldehyde addition of 1.2 mL had the best MB removal performance. By

microscopic morphological comparison, a shell-shaped structure appeared on the surface of CS-G/AC compared to AC. The characteristic peak of CS was observed at $2\theta = 10^\circ$, indicating the successful cross-linking of AC with CS. The quadratic regression model established by the response surface experiment was significant ($P < 0.05$), implying that the results could provide a technical reference for MB-containing wastewater treatment. CS-G/AC had excellent adsorption characteristics for MB, with a predicted Q_m of 300.75 mg g^{-1} . According to the analysis of the kinetics and isotherms models, physisorption and homogeneous adsorption were dominant. Furthermore, an electrostatic adsorption process existed. After multiple regenerations, CS-G/AC still performed well in MB adsorption. The CS-G/AC was assumed to be a promising material for treating MB-containing wastewater.

Acknowledgments

This project was funded by National Science Foundation of Heilongjiang Provincial of China (LH2019D002).

References

- [1] V. Katheresan, J. Kannedo, S.Y. Lau, Efficiency of various recent wastewater dye removal methods: a review, *J. Environ. Chem. Eng.*, 6 (2018) 4676–4697.

- [2] R. Al-Tohamy, S.S. Ali, F. Li, K.M. Okasha, Y.A.-G. Mahmoud, T. Elsamahy, H. Jiao, Y. Fu, J. Sun, A critical review on the treatment of dye-containing wastewater: ecotoxicological and health concerns of textile dyes and possible remediation approaches for environmental safety, *Ecotoxicol. Environ. Saf.*, 231 (2022) 113160, doi: 10.1016/j.ecoenv.2021.113160.
- [3] P. Xiao, L. An, D. Wu, The use of carbon materials in persulfate-based advanced oxidation processes: a review, *New Carbon Mater.*, 35 (2020) 667–683.
- [4] L. An, P. Xiao, Zero-valent iron/activated carbon micro-electrolysis to activate peroxydisulfate for efficient degradation of chlortetracycline in aqueous solution, *RSC Adv.*, 10 (2020) 19401–19409.
- [5] T.-H. Liou, M.-H. Lin, Preparation of mesoporous graphene oxide/SBA-15 hybrid nanoparticles as a potential adsorbent for removal of cationic dyes, *Desal. Water Treat.*, 155 (2019) 285–295.
- [6] J. Singh, A.S. Dhaliwal, Electrochemical and photocatalytic degradation of methylene blue by using rGO/AgNWs nanocomposite synthesized by electroplating on stainless steel, *J. Phys. Chem. Solids*, 160 (2022) 110358, doi: 10.1016/j.jpss.2021.110358.
- [7] G. Sharma, S. Sharma, A. Kumar, A. Al-Muhtaseb, Mu. Naushad, A.A. Ghfar, G.T. Mola, F.J. Stadler, Guar gum and its composites as potential materials for diverse applications: a review, *Carbohydr. Polym.*, 199 (2018) 534–545.
- [8] Z. Yang, M. Li, M. Yu, J. Huang, H. Xu, Y. Zhou, P. Song, R. Xu, A novel approach for methylene blue removal by calcium dodecyl sulfate enhanced precipitation and microbial flocculant GA1 flocculation, *Chem. Eng. J.*, 303 (2016) 1–13.
- [9] T.K. Sindhu, R. Pavithran, A. Vidhya, Design of 3D-supramolecular metal organic framework of zinc as photocatalyst for the degradation of methylene blue through advanced oxidation process, *J. Mol. Struct.*, 1245 (2021) 131039, doi: 10.1016/j.molstruc.2021.131039.
- [10] Y. Wang, J. Wang, G. Li, X. Geng, T. Hu, F. Liu, Reversible filtration redox of methylene blue in dimethylsulfoxide by manganese oxide loaded carbonaceous nanofibrous membrane through Fenton-like oxidation, *J. Colloid Interface Sci.*, 588 (2021) 436–445.
- [11] M. Zhang, X. Liu, W. Li, Z. Tan, Q. Wang, L. Zhang, Removal of toxic dyes from aqueous solutions by adsorption onto a novel activated carbon prepared from chestnut shell, *Desal. Water Treat.*, 222 (2021) 246–258.
- [12] N.U. Alamin, A.S. Khan, A. Nasrullah, J. Iqbal, Z. Ullah, I.U. Din, N. Muhammad, S.Z. Khan, Activated carbon-alginate beads impregnated with surfactant as sustainable adsorbent for efficient removal of methylene blue, *Int. J. Biol. Macromol.*, 176 (2021) 233–243.
- [13] V. Srivastava, A.K. Choubey, Investigation of adsorption of organic dyes present in wastewater using chitosan beads immobilized with biofabricated CuO nanoparticles, *J. Mol. Struct.*, 1242 (2021) 130749, doi: 10.1016/j.molstruc.2021.130749.
- [14] P. Sirajudheen, N.C. Poovathumkuzhi, S. Vigneshwaran, B.M. Chelaveettil, S. Meenakshi, Applications of chitin and chitosan based biomaterials for the adsorptive removal of textile dyes from water — a comprehensive review, *Carbohydr. Polym.*, 273 (2021) 118604, doi: 10.1016/j.carbpol.2021.118604.
- [15] M.J. Ahmed, B.H. Hameed, E.H. Hummadi, Review on recent progress in chitosan/chitin-carbonaceous material composites for the adsorption of water pollutants, *Carbohydr. Polym.*, 247 (2020) 116690, doi: 10.1016/j.carbpol.2020.116690.
- [16] I.M. Minisy, N.A. Salahuddin, M.M. Ayad, Adsorption of methylene blue onto chitosan–montmorillonite/polyaniline nanocomposite, *Appl. Clay Sci.*, 203 (2021) 105993, doi: 10.1016/j.clay.2021.105993.
- [17] J. Men, H. Shi, C. Dong, Y. Yang, Y. Han, R. Wang, Y. Zhang, T. Zhao, J. Li, Preparation of poly(sodium 4-styrene sulfonate) grafted magnetic chitosan microspheres for adsorption of cationic dyes, *Int. J. Biol. Macromol.*, 181 (2021) 810–823.
- [18] U.A. Toor, T.T. Duong, S.-Y. Ko, F. Hussain, S.-E. Oh, Optimization of Fenton process for removing TOC and color from swine wastewater using response surface method (RSM), *J. Environ. Manage.*, 279 (2021) 111625, doi: 10.1016/j.jenvman.2020.111625.
- [19] S. Karimifard, M.R. Alavi Moghaddam, Application of response surface methodology in physicochemical removal of dyes from wastewater: a critical review, *Sci. Total Environ.*, 640–641 (2018) 772–797.
- [20] P. Hnatukova, I. Kopecka, M. Pivokonsky, Adsorption of cellular peptides of *Microcystis aeruginosa* and two herbicides onto activated carbon: effect of surface charge and interactions, *Water Res.*, 45 (2011) 3359–3368.
- [21] K. Aziz, F. Aziz, R. Mamouni, L. Aziz, N. Saffaj, Engineering of highly Brachyichiton populneus shells@polyaniline biosorbent for efficient removal of pesticides from wastewater: optimization using BBD-RSM approach, *J. Mol. Liq.*, 346 (2021) 117092, doi: 10.1016/j.molliq.2021.117092.
- [22] J. Li, A. Bao, J. Chen, Y. Bao, A green route to CO₂ adsorption on biomass chitosan derived nitrogen-doped micropore-dominated carbon nanosheets by different activators, *J. Environ. Chem. Eng.*, 10 (2022) 107021, doi: 10.1016/j.jece.2021.107021.
- [23] S. Aslam, M. Asgher, N.A. Khan, M. Bilal, Immobilization of *Pleurotus nebrodensis* WC 850 laccase on glutaraldehyde cross-linked chitosan beads for enhanced biocatalytic degradation of textile dyes, *J. Water Process Eng.*, 40 (2021) 101971, doi: 10.1016/j.jwpe.2021.101971.
- [24] Y. Yu, D. Chen, S. Xie, Q. Sun, Z.-X. Zhang, G. Zeng, Adsorption behavior of carbamazepine on Zn-MOFs derived nanoporous carbons: defect enhancement, role of N doping and adsorption mechanism, *J. Environ. Chem. Eng.*, 10 (2022) 107660, doi: 10.1016/j.jece.2022.107660.
- [25] H. Motaghi, P. Arabkhani, M. Parvinnia, A. Asfaram, Simultaneous adsorption of cobalt ions, azo dye, and imidacloprid pesticide on the magnetic chitosan/activated carbon@UiO-66 bio-nanocomposite: optimization, mechanisms, regeneration, and application, *Sep. Purif. Technol.*, 284 (2022) 120258, doi: 10.1016/j.seppur.2021.120258.
- [26] I.O. Saheed, W.-D. Oh, F.B.M. Suah, Removal of 1-butyl-3-methylimidazolium bromide from an aqueous solution by using a spongy chitosan-activated carbon composite, *Colloid Interface Sci. Commun.*, 42 (2021) 100393, doi: 10.1016/j.colcom.2021.100393.
- [27] C. Huang, H. Liao, X. Ma, M. Xiao, X. Liu, S. Gong, X. Shu, X. Zhou, Adsorption performance of chitosan Schiff base towards anionic dyes: electrostatic interaction effects, *Chem. Phys. Lett.*, 780 (2021) 138958, doi: 10.1016/j.cplett.2021.138958.
- [28] X. Sun, H. Qi, S. Mao, Z. Sun, Atrazine removal by peroxy-monosulfate activated with magnetic CoFe alloy@N-doped graphitic carbon encapsulated in chitosan carbonized microspheres, *Chem. Eng. J.*, 423 (2021) 130169, doi: 10.1016/j.cej.2021.130169.
- [29] M. Wang, Y. Luo, P. Yu, Treatment of copper-containing wastewater with chitosan-modified activated carbon fiber mats, *Ind. Water Treat.*, 39 (2019) 62–66.
- [30] J. Xu, Y. Chen, H. Ye, J. Zhang, J. Zhang, Z. Luo, Synthesis, characterization and physicochemical properties study of oxadiazole co-crystals, *CIESC J.*, 71 (2020) 1851–1858.
- [31] A. Valencia, R. Muñoz-Valencia, S.G. Ceballos-Magaña, C.K. Rojas-Mayorga, A. Bonilla-Petriciolet, J. González, I.A. Aguayo-Villarreal, Cyclohexane and benzene separation by fixed-bed adsorption on activated carbons prepared from coconut shell, *Environ. Technol. Innovation*, 25 (2022) 102076, doi: 10.1016/j.eti.2021.102076.
- [32] A. Beta Daniel, D. Aruldas, S. Balachandran, J. George, I.H. Joe, Spectroscopic investigation, Hirshfeld surface analysis and molecular docking studies on mebendazole and its derivatives, *J. Mol. Struct.*, 1227 (2021) 129566, doi: 10.1016/j.molstruc.2020.129566.
- [33] H. Grabi, A. Ouakouak, S. Kadouche, W. Lemlikchi, F. Derridj, A.T.M. Din, Mechanism and adsorptive performance of ash tree seeds as a novel biosorbent for the elimination of methylene blue dye from water media, *Surf. Interfaces*, 30 (2022) 101947, doi: 10.1016/j.surfin.2022.101947.
- [34] E.A. Idohou, J.K. Fatombi, S.A. Osseni, I. Agani, D. Neumeyer, M. Verelst, R. Mauricot, T. Aminou, Preparation of activated

- carbon/chitosan/Carica papaya seeds composite for efficient adsorption of cationic dye from aqueous solution, *Surf. Interfaces*, 21 (2020) 100741, doi: 10.1016/j.surf.2020.100741.
- [35] W. Liu, H. Xie, J. Zhang, C. Zhang, Sorption removal of cephalixin by HNO₃ and H₂O₂ oxidized activated carbons, *Sci. China Chem.*, 55 (2012) 1959–1967.
- [36] C. Santhosh, E. Daneshvar, P. Kollu, S. Peräniemi, A.N. Grace, A. Bhatnagar, Magnetic SiO₂@CoFe₂O₄ nanoparticles decorated on graphene oxide as efficient adsorbents for the removal of anionic pollutants from water, *Chem. Eng. J.*, 322 (2017) 472–487, doi: 10.1016/j.seppur.2021.119193.
- [37] M.-C. Sparenberg, B. Hanot, C. Molina-Fernández, P. Luis, Experimental mass transfer comparison between vacuum and direct contact membrane distillation for the concentration of carbonate solutions, *Sep. Purif. Technol.*, 275 (2021) 119193, doi: 10.1016/j.seppur.2021.119193.
- [38] W. Plazinski, W. Rudzinski, A. Plazinska, Theoretical models of sorption kinetics including a surface reaction mechanism: a review, *Adv. Colloid Interface Sci.*, 152 (2009) 2–13.
- [39] J. Zhang, Physical insights into kinetic models of adsorption, *Sep. Purif. Technol.*, 29 (2019) 115832, doi: 10.1016/j.seppur.2019.115832.
- [40] H. Swenson, N.P. Stadie, Langmuir's theory of adsorption: a centennial review, *Langmuir*, 35 (2019) 5409–5426.
- [41] C. Na, Size-controlled capacity and isocapacity concentration in Freundlich adsorption, *ACS Omega*, 5 (2020) 13130–13135.
- [42] M. Ruthiraan, E.C. Abdullah, N.M. Mubarak, S. Nizamuddin, Adsorptive removal of methylene blue using magnetic biochar derived from agricultural waste biomass: equilibrium, isotherm, kinetic study, *Int. J. Nanosci.*, 17 (2018) 1850002, doi: 10.1142/S0219581X18500023.
- [43] T.F. Schmidt, K.A. Riske, L. Caseli, C. Salesse, Dengue fusion peptide in Langmuir monolayers: a binding parameter study, *Biophys. Chem.*, 271 (2021) 106553, doi: 10.1016/j.bpc.2021.106553.
- [44] M. Minisy, N.A. Salahuddin, M.M. Ayad, Chitosan/polyaniline hybrid for the removal of cationic and anionic dyes from aqueous solutions, *J. Appl. Polym. Sci.*, 136 (2018) 47056, doi: 10.1002/app.47056.
- [45] S. Sabar, H. Abdul Aziz, N.H. Yusof, S. Subramaniam, K.Y. Foo, L.D. Wilson, H.K. Lee, Preparation of sulfonated chitosan for enhanced adsorption of methylene blue from aqueous solution, *React. Funct. Polym.*, 151 (2020) 104584, doi: 10.1016/j.reactfunctpolym.2020.104584.
- [46] W. Liu, Q. Ren, R. Wu, B. Wang, Y. Hu, Q. Hu, Y. Ni, Insight on adsorption of cellulase on wet ground corncob residues and its evaluation by multivariate linear analysis, *Bioresour. Technol.*, 318 (2020) 124107, doi: 10.1016/j.biortech.2020.124107.
- [47] N.N.A. Malek, A.H. Jawad, A.S. Abdulhameed, K. Ismail, B.H. Hameed, New magnetic Schiff's base-chitosan-glyoxal/fly ash/Fe₃O₄ biocomposite for the removal of anionic azo dye: an optimized process, *Int. J. Biol. Macromol.*, 146 (2020) 530–539.
- [48] R. Foroutan, R. Mohammadi, J. Razeghi, B. Ramavandi, Performance of algal activated carbon/Fe₃O₄ magnetic composite for cationic dyes removal from aqueous solutions, *Algal Res.*, 40 (2019) 101509, doi: 10.1016/j.algal.2019.101509.
- [49] M. Wu, Q. Guo, G. Fu, Preparation and characteristics of medicinal activated carbon powders by CO₂ activation of peanut shells, *Powder Technol.*, 247 (2013) 188–196.
- [50] Z. Ding, Y. Wan, X. Hu, S. Wang, A.R. Zimmerman, B. Gao, Sorption of lead and methylene blue onto hickory biochars from different pyrolysis temperatures: Importance of physicochemical properties, *J. Ind. Eng. Chem.*, 37 (2016) 261–267.
- [51] C. Wang, R. Ma, Z. Huang, X. Liu, T. Wang, K. Chen, Preparation and characterization of carboxymethylcellulose based citric acid cross-linked magnetic aerogel as an efficient dye adsorbent, *Int. J. Biol. Macromol.*, 181 (2021) 1030–1038.
- [52] Y. Mu, H. Ma, NaOH-modified mesoporous biochar derived from tea residue for methylene blue and Orange II removal, *Chem. Eng. Res. Des.*, 167 (2021) 129–140.
- [53] A.H. Jawad, A.S. Abdulhameed, Mesoporous Iraqi red kaolin clay as an efficient adsorbent for methylene blue dye: adsorption kinetic, isotherm and mechanism study, *Surf. Interfaces*, 18 (2020) 100422, doi: 10.1016/j.surf.2019.100422.
- [54] S. Sharma, G. Sharma, A. Kumar, T.S. AlGarni, Mu. Naushad, Z.A. AlOthman, F.J. Stadler, Adsorption of cationic dyes onto carrageenan and itaconic acid-based superabsorbent hydrogel: synthesis, characterization and isotherm analysis, *J. Hazard. Mater.*, 421 (2022) 126729, doi: 10.1016/j.jhazmat.2021.126729.